

# Lawrence Berkeley National Laboratory

## Recent Work

### Title

In situ study of rotating lattice single-crystal formation in Sb<sub>2</sub>S<sub>3</sub> glass by Laue  $\mu$ XRD

### Permalink

<https://escholarship.org/uc/item/3z8823tz>

### Journal

Journal of the American Ceramic Society, 103(7)

### ISSN

0002-7820

### Authors

Au-Yeung, C  
Stan, C  
Tamura, N  
et al.

### Publication Date






2020-07-01

### DOI

10.1111/jace.16905

Peer reviewed

## SPECIAL ISSUE ARTICLE

In situ study of rotating lattice single-crystal formation in  $\text{Sb}_2\text{S}_3$  glass by Laue  $\mu\text{XRD}$ Courtney Au-Yeung<sup>1</sup>  | Camelia Stan<sup>2</sup>  | Nobumichi Tamura<sup>2</sup>  | Himanshu Jain<sup>3</sup>  | Volkmar Dierolf<sup>1</sup> <sup>1</sup>Physics Department, Lehigh University, Bethlehem, PA, USA<sup>2</sup>Lawrence Berkeley National Laboratory, Berkeley, CA, USA<sup>3</sup>Materials Science and Engineering Department, Lehigh University, Bethlehem, PA, USA

## Correspondence

Volkmar Dierolf, Physics Department, Lehigh University, 16 Memorial Drive East, Bethlehem, PA 18015, USA.  
Email: vod2@lehigh.edu

## Present address

Camelia Stan, Lawrence Livermore National Laboratory, Livermore, CA, USA

## Funding information

Department of Energy, Grant/Award Number: DE SC0005010; National Science Foundation, Grant/Award Number: DGE-1452783

## Abstract

Single-crystal architectures in glass, formed by a solid-solid transformation via laser heating, are novel solids with a rotating lattice. To understand the process of lattice formation that proceeds via crystal growth, we have observed in situ  $\text{Sb}_2\text{S}_3$  crystal formation under X-ray irradiation with simultaneous Laue micro X-ray diffraction ( $\mu\text{XRD}$ ) pattern collection. By translating the sample with respect to the beam, we form rotating lattice single (RLS) crystal lines with a consistently linear relationship between the rotation angle and distance from nucleation site. The lines begin with a seed crystal, followed by a transition region comprising of sub-grain or very similarly oriented grains, followed by the presence of a rotating lattice single crystal of unrestricted length. The results demonstrate that the primary cause of lattice rotation within RLS crystals is the densification accompanying the glass  $\rightarrow$  crystal transformation, rather than stresses produced from the difference in thermal expansion coefficient of the two phases or paraelectric  $\rightarrow$  ferroelectric transition during cooling to ambient temperature.

## KEYWORDS

chalcogenides, crystal growth, crystals/crystallization, X-ray methods

## 1 | INTRODUCTION

Laser-induced crystallization is a novel method to fabricate single-crystal architectures within glass.<sup>1</sup> Laser-heating is spatially selective and offers an opportunity to fabricate crystalline architectures in glass with amorphous-crystalline interfaces. An amorphous phase can be directly converted into a single crystal by a solid-solid phase transformation via space-selective laser heating of glass in which the sample does not melt during crystal fabrication, as demonstrated recently for chalcogenide glass systems.<sup>2</sup> By only locally heating the glass to include nucleation, specific crystal geometries can be created in the bulk glass sample. Antimony trisulfide ( $\text{Sb}_2\text{S}_3$ ) crystals are particularly attractive due to their piezoelectric and ferroelectric properties and transparency for the infrared

wavelengths.<sup>3</sup> Due to such properties,  $\text{Sb}_2\text{S}_3$  has practical applications in energy storage, photovoltaics, and thermoelectric and optoelectronic devices.<sup>4–8</sup>

Prior work focused on crystallization of Sb–S–I glasses using a continuous wave (CW) laser to create single crystal architectures in glass (SCAG) at or near the surface. In these glass systems, we have created single crystal dots (0D), crystal lines (1D), and 2D planar structures.<sup>9,10</sup> Electron backscatter diffraction (EBSD) mapping of 1D crystal lines indicates that these single crystal architectures grow in a straight line, while simultaneously rotating gradually about an axis that is parallel to glass surface and normal to growth direction. Ex situ experiments have been used to study the formation of these rotating lattice single (RLS) crystals,<sup>9,10</sup> which are particularly interesting because only the lattice rotates while the crystal's macroscopic shape is maintained.<sup>10</sup> Note that RLS

crystal is comprised of a new type of lattice, which is derived from perfect single-crystal lattice by adding a rotational element to translational symmetry. Controlling this rotating lattice is key for exploiting these novel crystals in applications. The driving force and the stage when the lattice rotates are unknown at present. Specifically, it is unclear if the rotation occurs due to thermal expansion mismatch, the paraelectric to ferroelectric transition during cooling, or stresses generated as a result of crystallization itself. Crystal formation and growth are dynamic in nature, therefore real time measurements are necessary to fully understand the processes that eventually control the rate of rotation and the corresponding properties of RLS crystals. This was the goal of work that we report in this paper.

To this end, we observe crystallization and growth in Sb–S–I glass in real time by using a white synchrotron X-ray beam as a spatially selective heating source while simultaneously collecting time-resolved diffraction patterns. The measurements are made while translating the sample, enabling us to observe the formation of a crystal with a rotation lattice similar to the ones produced with a CW laser.<sup>2,9</sup> X-ray diffraction has previously been used to observe the nucleation and growth of crystals in solutions,<sup>11,12</sup> within a melt,<sup>13</sup> and in thin films,<sup>14</sup> Micro X-ray diffraction,  $\mu$ XRD, is commonly used to identify and characterize materials at a micron- and sub-micron scale to analyze spatial distribution of phases, structure, strain and stress, and/or plastic deformation inside the sample.<sup>15</sup> However, this is the first time that an X-ray source has been used to investigate the formation of crystals on the surface of bulk glass. These real time observations provide insight into the underlying mechanism responsible for enabling the rotating crystal lattice.

## 2 | EXPERIMENTAL PROCEDURES

Single-crystal architecture in Sb–S–I glasses is most conveniently fabricated with a CW laser. To create a similar crystal fabrication environment while simultaneously collecting lattice characterization data, we used a white synchrotron X-ray beam. To eliminate complexity from compositional changes, long range diffusion etc, we focused on the congruent growth of  $\text{Sb}_2\text{S}_3$  crystals on the surface of  $\text{Sb}_2\text{S}_3$  glass. These experiments were performed at beamline 12.3.2 of the Advanced Light Source at Lawrence Berkeley National Laboratory. A white X-ray beam ( $\sim 5\text{--}24$  keV) was focused to a  $1 \times 1 \mu\text{m}^2$  spot size (measured in transmission) using a pair of Kirkpatrick-Baez mirrors. The sample is mounted at  $45^\circ$  to the X-ray beam and is controlled using high precision XYZ translation stages. Laue diffraction patterns were collected using a DECTRIS Pilatus 1M detector at a rate of 20–30 patterns per second to observe crystallization in real time. A schematic diagram of the

experimental set up is shown in Figure 1. Quantitative information was extracted from the Laue patterns using the in-house X-ray microdiffraction analysis software package XMAS.<sup>15</sup>

To fabricate single crystals using the X-ray beam, a low-power diode laser was first used to focus the beam on the surface of the sample. It calibrated the focus without exposing the sample to the X-ray beam to eliminate the possibility of damaging the sample during the set up. The intensity of the X-ray beam was controlled by adjusting a pair of slits to cut off more or less of the impinging X-ray beam. Beam intensity was measured using an ion counter mounted between the optics chamber and the sample. The intensities used for crystallization were between 3500 and 11 000 counts with the best results around 8000 counts. We found that at  $<7800$  counts, the heat load was often insufficient to cause crystallization, whereas  $>9000$  counts led to the undesirable formation of multiple grains. All crystals discussed in this paper were created at the optimal intensity of 8000–8200 counts, which equates to a measured flux value of approximately  $94.11 \times 10^{22}$  photons/s/ $\text{m}^2$ . To determine whether sample temperature affects nucleation and/or crystallization, an Anton-Paar DHS 900 heating stage was used to heat the samples up to  $100^\circ\text{C}$ , well below the  $\text{Sb}_2\text{S}_3$  crystallization temperature of  $190^\circ\text{C}$ .<sup>16</sup>

In order to minimize oxidation, we proactively placed Kapton tape, which was transparent to the X-ray source, over the sample, and nitrogen was continuously flowed over the surface. To confirm that the X-ray beam crystallization did not produce oxidation effects as seen with traditional laser crystallization, crystals were formed both in air and under a nitrogen filled environment. There were no differences in crystal diffraction patterns collected between the two environments,

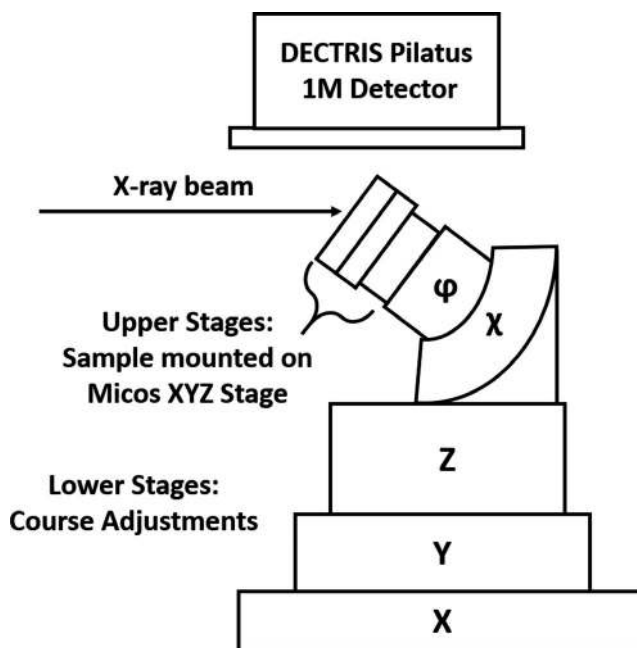


FIGURE 1 Schematic diagram of experimental set up

thus confirming that the X-ray beam did not produce oxidation effects during crystallization. This may be due to the CW laser producing a higher temperature on the surface of the sample compared to the X-ray beam.

### 3 | RESULTS

Our first objective was to determine whether it is possible to fabricate crystals using the X-ray beam. To test this option, we exposed the crystal to an X-ray beam and measured diffraction every 0.05 seconds over a total of 5 minutes, with  $t = 0$  being the point when exposure first began. Since glass is amorphous, the appearance of a diffraction pattern would indicate crystallization in the sample. The high time resolution of the detector allowed us to observe changes within the crystal lattice during initial growth. Using the XMAS software, each diffraction pattern was indexed to determine the single crystal orientation as a function of time.

We first created crystal dots that would serve as seed crystals for other crystal structures, such as lines and 2D architectures. After a seed crystal was created, the sample was re-exposed to the X-ray beam while simultaneously translating the sample stage relative to the X-ray beam to create a crystal line. Temperature of heating stage, translation velocity, and beam intensity were varied in order to determine optimal parameters for line crystallization (see Table 1). Exposure time in Table 1 refers to the total time the sample was exposed to the X-ray beam for crystallization. All experiments considered here were performed under an  $N_2$  environment under Kapton to avoid potential oxidation.

Figure 2 displays an indexed reflection pattern, where 93 peaks were identified and indexed as one  $Sb_2S_3$  crystal. The XMAS software calculates a variety of crystal parameters that define the orientation and characteristics of the crystal lattice. Indexation of the resulting Laue patterns shows that the crystal lattice rotates in the X-ray scanning direction for all samples, consistent with results from laser fabrication.<sup>9,10</sup> The rotation rates were calculated using the orientation of the crystal c-axis relative to the surface normal. In 15 of 19 samples, we find that the rotation rate is linear with respect to translation distance. The four unsuccessful samples contained three lines that failed to crystallize and therefore either contained a low number of indexed frames, less than 30 frames detecting over six indexed peaks, and one crystal line was crossed through previously existing crystal lines causing a polycrystalline line that contained a new starting orientation each time that the line passed through an existing crystal line. These crystals may have failed to grow as a single-crystal line due to defects in the glass such as deep scratches or fluctuations in beam intensity. Initial analysis of the rotation rate calculated the average rotation of samples at 22°C, 70°C,

**TABLE 1** Experimental parameters used for generating crystal lines

Sample	Exposure time (s)	Temperature (°C)	Translation velocity ( $\mu\text{m/s}$ )
Fastline 1	99.99	70	1
Fastline 2	99.99	70	1
Fastline 3	99.99	70	1
Fastline 4	50.01	70	2
Fastline 5	50.01	70	2
Fastline 6	50.01	70	2
Fastline 7	24.99	70	4
Fastline 8	24.99	70	4
Fastline 10	99.99	70	4
Fastline 11	99.99	80	1
Fastline 12	99.99	80	1
Fastline 13	99.99	80	1
Fastline 14	50.01	80	2
Fastline 15	50.01	80	2
Fastline 16	24.99	80	4
Fastline 17	63	22	4
Fastline 18	99.99	22	1
Fastline 19	50.01	22	2
Fastline 20	50.01	22	2

and 80°C were 0.0289, 0.0336, and 0.0214°/ $\mu\text{m}$ , respectively. When analyzing the effects of the writing speed, 1, 2, and 4  $\mu\text{m/s}$ , we found mean rotation rates of 0.0181, 0.0272, and 0.0430°/ $\mu\text{m}$ .

Let us focus, as an example, on a specific line, fastline8, to explore the crystallization process and whether its evolution with time is similar to the rotation that we observe in laser fabricated crystals.<sup>9,10</sup> Fastline8 displays similar phenomena shown in each single crystal line, so it is very appropriate to further characterize the mechanisms of the rotating lattice formation. When observing the diffraction patterns, we can see that the entire crystal diffraction pattern rotates in the direction that the stage is translated, to the right for fastline8 (Video S1).

During initial growth of the crystal line, we observe a transition from the crystal dot seed to the start of the crystal line where there is a gap in the indexed patterns. As reported previously,<sup>16</sup> there is transition region between the seed crystal and the rest of the line that exhibits additional complexity. This region is prone to the formation of defects that can cause higher angle boundaries during crystallization, leading to undesirable additional grain formation as the growth front extends from the crystal seed to begin to form the line.<sup>17</sup> It occurs due to competition between growth of the existing crystal seed and nucleation of potential new crystal seeds.<sup>17</sup> If growth during this area is inhibited, the diffraction patterns

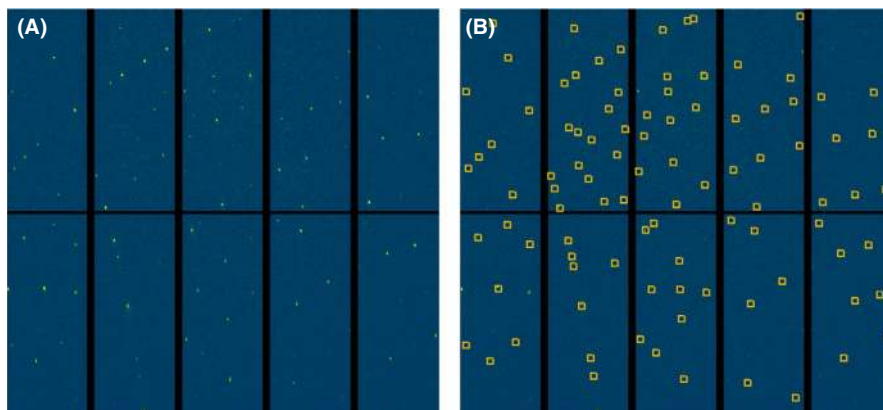


**FIGURE 2** A, Laue pattern of crystal before indexation. B, Laue pattern with box indexation, each box represents an identified crystal reflection

would not be as strong, resulting in a low number of indexed Laue spots. Figure 3 shows the deviation angle as a function of distance from the center of the seed, and selected diffraction patterns throughout.

There is a linear relationship between the deviation angle and translation distance, as observed in all of our experiments. In Figure 3B representing the transition zone at 15  $\mu\text{m}$ , the pattern appears doubled, vs the patterns at 0.12 and 99.84  $\mu\text{m}$ . The spots at 15  $\mu\text{m}$  are more diffused and doubled when compared to the beginning and end of the line. We observe that a second grain with almost the same orientation forms, at 7.2  $\mu\text{m}$ , and becomes the dominant and singular grain for the rotation after some distance from the original seed, at 19.8  $\mu\text{m}$ . In this transition zone, the crystallographic data was misfit by XMAS due to weak diffraction scattering or doubling of the lattice, signifying the presence of two sub-grains of approximately

equal diffracting volume, as discussed above. We do not see any other grain orientations form throughout the translation of the sample, and the overall trend in rotation remains linear. To confirm that we have a singular grain beyond the transition region, we compared the number of peaks indexed as a single crystal to the total number of peaks. At 99.84  $\mu\text{m}$ , 98% of peaks were indexed as belonging to a single grain compared to the transition zone at 15  $\mu\text{m}$ , where only 13% of peaks were identified as a single grain indicating that it is polycrystalline at this zone. It appears that sub-grains or a highly oriented polycrystalline structure forms during the “transition zone” between the seed and single crystal line; after this zone we observe throughout a rotating-lattice single crystal line. For this crystal line, we measure a constant rate of rotation in the growth direction, similar to that previously reported for ex situ laser formed rotating-lattice-single crystals,<sup>9,10</sup> but now in real

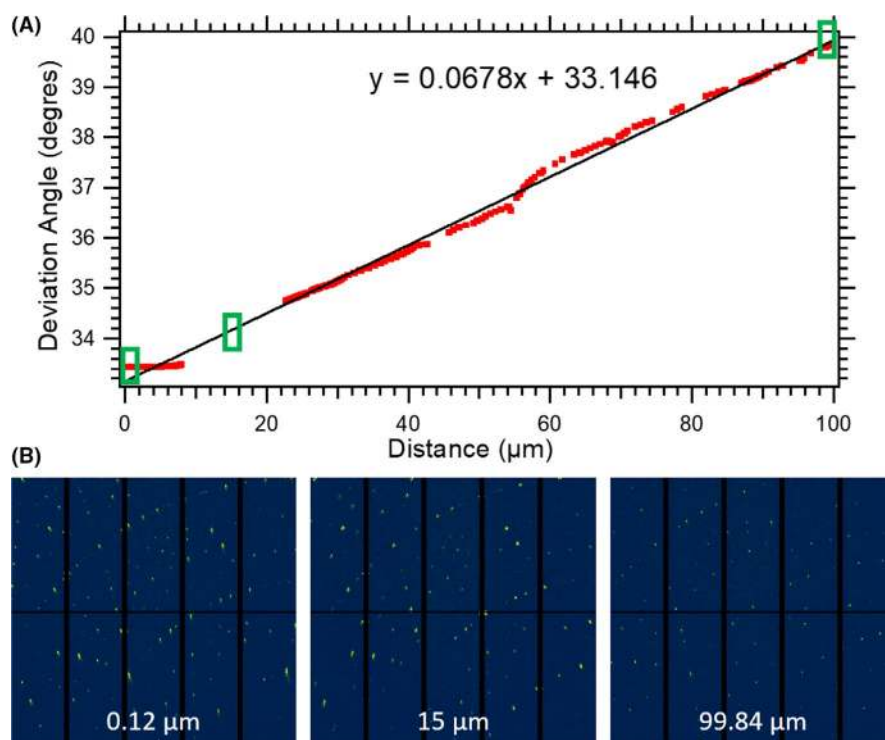


**FIGURE 3** A, Plot of the deviation angle vs distance from the crystal seed. The equation of the linear fit is shown within the graph. B, Laue patterns at 0.12, 15, and 99.84  $\mu\text{m}$ , which coincide with the green rectangles in (A)



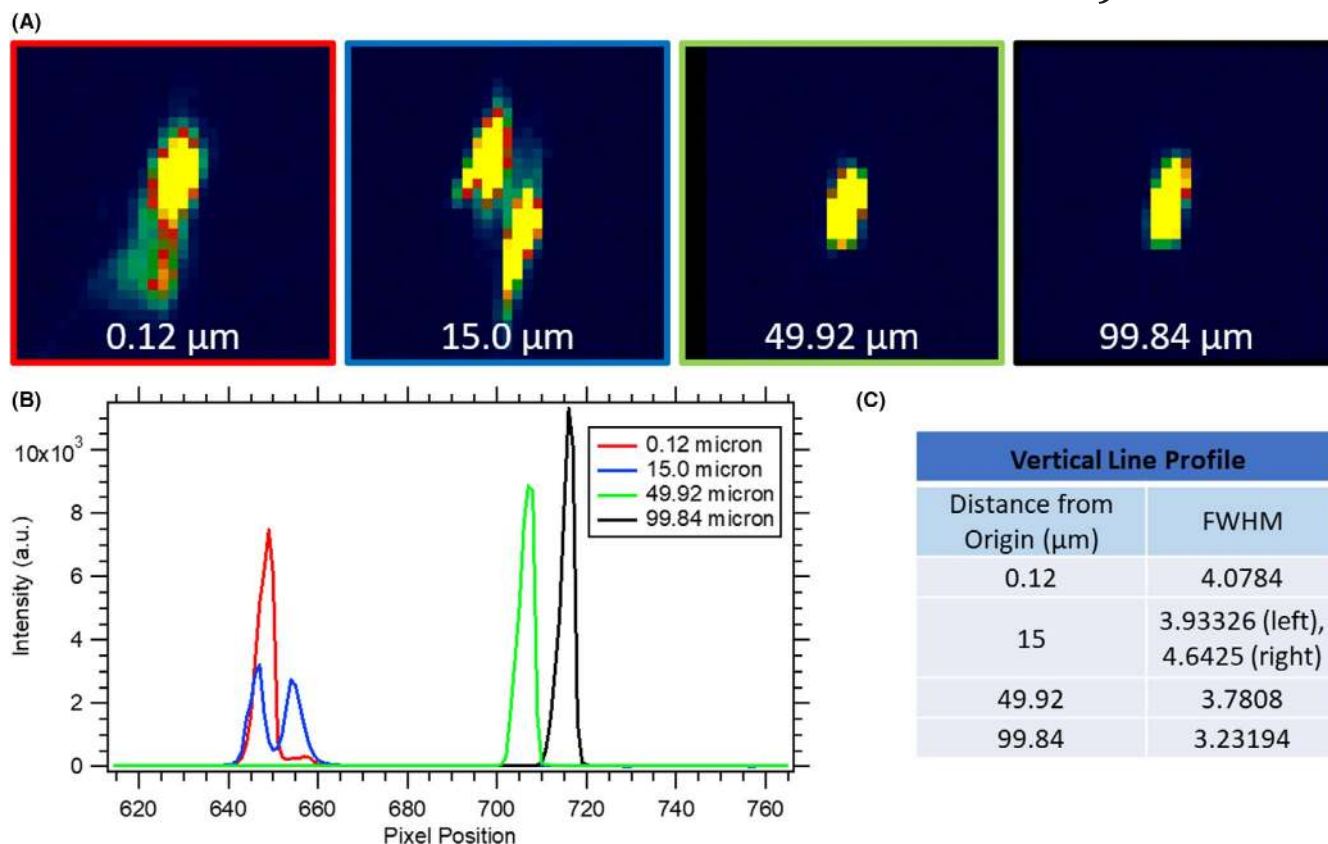


**FIGURE 4** A, Selected reflection  $(-9, 6, 3)$  at different distances of the crystal line. B, Line profiles of each reflection plotted as pixel position vs intensity. C, Table including the full width half maximum of each Laue diffraction spot

time. The lattice rotates at  $0.0687^\circ/\mu\text{m}$  along the growth direction of the crystal line.

Reflection  $(-9, 6, 3)$  was tracked in detail as a function of time for the same crystal line, fastline8, to further understand the rotating lattice (Figure 4). The reflection's angle changes, which is consistent with a rotation of the lattice as described previously. We also observe a change in the shape of the reflection over time. At  $0.12 \mu\text{m}$ , still in the crystal seed, the reflection appears smeared relative to an ideal 2D Gaussian profile. Within the transition zone, a second  $(-9, 6, 3)$  reflection appears, indicative of the presence of a second grain with a very low angle grain boundary. Here a competition appears to develop between the growth of the original grain and the nucleation of additional ones. In the case of fastline8, the second reflection persists beyond the transition zone, whereas the original one disappears. It indicates that the second grain, whose initial orientation is very similar to that of the original one, is the singular grain that continues to grow and rotate throughout the line. We see that as the sample is translated and the crystal line continues to grow, at  $49.92$  and  $99.84 \mu\text{m}$ , only one reflection is present indicating a single-crystal grain.

To further quantify the observations, the intensity across the center of the Laue reflection is plotted at four different distances (Figure 4B). At  $0.12 \mu\text{m}$ , there is one main peak

with a shoulder, possibly the initiation of a second grain. This main peak and shoulder split, eventually becoming two peaks that are of similar intensity at  $15.0 \mu\text{m}$  before merging again to a single peak of higher intensity. During this region, smaller crystal grains may be beginning to form but the intensity of each of these peaks is marginally less than that of the “main peak.” It is also worth noting that after the Laue reflections merge into a single peak, the intensity of that peak increases as the crystal line is written. The full width at half the maximum decreases, indicating that the peak does narrow over time (Figure 4C).

In the full Laue diffraction pattern of fastline8 taken at 12.48 seconds, that is,  $49.92 \mu\text{m}$  from the seed, 113 peaks were correctly indexed as one  $\text{Sb}_2\text{S}_3$  crystal (Figure 5). Closer inspection of selected individual diffraction peaks, such as  $(-12, 6, 15)$  and  $(-12, 6, 6)$ , show that they have the same slightly smeared shape that we observed in ex-situ experiments of our previously laser-crystallized samples.<sup>9,10</sup>

## 4 | DISCUSSION

How crystal architectures form within an amorphous matrix is mostly unknown at present.<sup>18,19</sup> Using in situ heating of

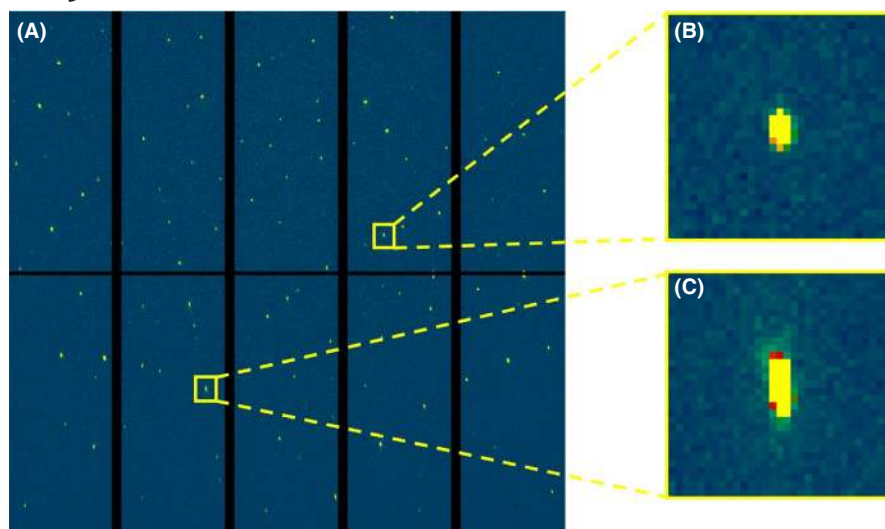


**FIGURE 5** A, Laue diffraction pattern from an X-ray fabricated  $\text{Sb}_2\text{S}_3$  single crystal. B, Selected reflection  $(-12, 6, 15)$  extracted from the Laue pattern. C, Selected reflection  $(-12, 6, 6)$  extracted from the Laue pattern

glass by X-ray beam, we observed the evolution of congruent crystallization in  $\text{Sb}_2\text{S}_3$  glass and tracked changes in orientation in real time, providing an insight into the origin of recently discovered rotating-lattice-single crystals. We fabricated lines starting from previously formed seed crystal dots. We observed a smooth rotation of the single-crystal lattice as the lines were forming, in agreement with previously reported ex situ observations.<sup>9</sup> During this rotation, the diffraction pattern indicates that the lattice rotates in the plane of the sample translation. Since the X-ray beam is the probe beam for diffraction as well as the source for crystallization, the diffraction patterns are being recorded at the growth front of the crystal line. If the rotation occurred at a later time, it would not be observed during the in situ data collection. Thus, we can conclude that the rotation is occurring during growth at the growth front, rather than subsequently behind the growth front.

When crystals are plastically strained, their Laue diffraction spots display significant spreading.<sup>20</sup> Plastic deformation introduces unpaired dislocations and small-angle tilt boundaries, in addition to residual elastic strain. When sufficiently mobile, the unpaired dislocations arrange to create tilt dislocation walls.<sup>21,22</sup> One major characteristic of these diffraction patterns is that the individual Laue spots are smeared and elliptical in nature rather than a Gaussian profile that is associated with a “perfect” single crystal. The smeared spots that we observe in our Laue patterns are similar to those of plastically deformed crystals. So they are likely from a similar distribution of dislocations and uniform elastic bending strain, but their origin is not plastic deformation; they arise from accommodation of stresses from the densification of the sample during glass to crystal transformation and crystal growth.<sup>9,23</sup> This introduction of random and well organized arrangement of dislocations is believed to be the source of lattice rotation of the RLS crystals.

The present results are consistent with previous results in that the rotation is likely due to the inclusion of dislocations

to accommodate stresses.<sup>9</sup> Furthermore, these in situ observations establish that these stresses arise primarily from the difference in density of the  $\text{Sb}_2\text{S}_3$  glass and crystal phases, 4.33 and 4.562 g/cm<sup>3</sup>, respectively. As proposed by Savvitskii et al,<sup>9</sup> the densification during devitrification on the surface produces asymmetric tensile stress on the crystal side of the interface, which will be the primary cause of systematic lattice rotation. Since the measurements were made at about the temperature of crystal growth, stresses from the difference in thermal expansion coefficients of the crystal and glass phases will be negligible, and they cannot be the source of lattice rotation. Likewise, stresses from paraelectric to ferroelectric phase transition upon cooling are absent during in situ measurements and cannot contribute to the lattice rotation observed here.

Initial analysis of average rotation rates for the translation speed was discussed above. We observed that the rotation rate increased when the translation speed was increased. If the rotation occurs due to dislocations within the lattice, a slower translation speed could lead to relaxation of stresses in neighboring glass thereby letting the dislocations anneal out and result in a smaller observed rate of rotation. To further explore this phenomenon, future studies with a larger parameter space and sample size need to be performed to confirm these effects.

In every single-crystal line fabricated, there is a “transition zone” at the boundary between the initial seed and the rest of the line, where the diffraction patterns are diffused, and some reflections appear doubled and/or smeared. This “doubling” could be the result of either a secondary grain forming in this region, or dislocations forming in the existing grain aligning to create that produce this doubled reflection. This region is poorly indexed for all lines. The transition zone is followed by the rest of the line, whose rotation rate is linear with respect to distance. Overall, the rotation stays consistently linear from the seed crystal to the end of the crystal line. The diffraction

peaks become sharper with increasing distance from the seed, although they remain elliptical in profile. This is the characteristic of a curved crystal plane, and often occurs from dislocations piling up to eventually cause a low-angle boundary.<sup>23</sup> These results support the model that lattice rotation in RLS crystal arises from the presence of unpaired dislocations and small-angle boundaries.

## 5 | CONCLUSIONS

In this novel experiment, we observed the growth of rotating lattice single  $\text{Sb}_2\text{S}_3$  crystal lines in  $\text{Sb}_2\text{S}_3$  glass in situ in real time using micro X-ray diffraction. We found that the lattice rotation occurs during growth and remains constant along most of the crystal line. The rotation rate increases with increasing crystal translation speed. The crystal lines contain a poorly single-crystalline region between the seed dot and the rest of the line but remain a single crystal beyond this region. The elliptical nature of the Laue diffraction spots confirm previous models that dislocations are the underlying mechanism of these RLS crystals.<sup>9</sup> These dislocations, and thus lattice rotation, are produced at the growth interface primarily in response to increase in density accompanying the glass to crystal transformation. Finally, in situ  $\mu\text{XRD}$  has been proven to be a powerful tool to determine the nature of crystal growth when creating single crystal architectures in glass.

## ACKNOWLEDGMENTS

This work was supported by the Basic Energy Sciences Division, Department of Energy (project DE SC0005010). CA was supported by a National Science Foundation Graduate Research Fellowship (Grant No. DGE-1452783).  $\mu\text{XRD}$  measurements were made at the Advanced Light Source, which is a DOE Office of Science User Facility under contract no. DE-AC02-05CH11231. CS acknowledges the support of the US Department of Energy through Lawrence Livermore National Laboratory under contract, DE-AC52-07NA27344.

## ORCID

Courtney Au-Yeung  <https://orcid.org/0000-0001-5163-2479>  
Camelia Stan  <https://orcid.org/0000-0002-5025-5568>  
Nobumichi Tamura  <https://orcid.org/0000-0002-3698-2611>  
Himanshu Jain  <http://orcid.org/0000-0003-4382-9460>  
Volkmar Dierolf  <https://orcid.org/0000-0003-0528-7162>

## REFERENCES

- Stone A, Jain H, Dierolf V, Sakakura M, Shimotsuma Y, Miura K, et al. Direct laser-writing of ferroelectric single-crystal waveguide architectures in glass for 3D integrated optics. *Sci Rep*. 2015;19(5):10391.
- Savytskii D, Knorr B, Dierolf V, Jain H. Demonstration of single crystal growth via solid-solid transformation of a glass. *Sci Rep*. 2016;18(6):23324.
- Varghese J, Barth S, Keeney L, Whatmore RW, Holmes JD. Nanoscale ferroelectric and piezoelectric properties of  $\text{Sb}_2\text{S}_3$  nanowire arrays. *Nano Lett*. 2012;12(2):868–72.
- Rajpure KY, Bhosale CH.  $\text{Sb}_2\text{S}_3$  semiconductor-septum rechargeable storage cell. *Mater Chem Phys*. 2000;64(1):70–4.
- Kim D-H, Lee S-J, Park MS, Kang J-K, Heo JH, Im SH, et al. Highly reproducible planar  $\text{Sb}_2\text{S}_3$ -sensitized solar cells based on atomic layer deposition. *Nanoscale*. 2014;6(23):14549–54.
- Geng ZR, Wang MX, Yue GH, Yan PX. Growth of single-crystal  $\text{Sb}_2\text{S}_3$  nanowires via solvothermal route. *J Cryst Growth*. 2008;310(2):341–4.
- Wang G, Cheung CL. Building crystalline  $\text{Sb}_2\text{S}_3$  nanowire dandelions with multiple crystal splitting motif. *Mater Lett*. 2012;67(1):222–5.
- Kondrotas R, Chen C, Tang J.  $\text{Sb}_2\text{S}_3$  solar cells. *Joule*. 2018;2(5):857–78.
- Savytskii D, Jain H, Tamura N, Dierolf V. Rotating lattice single crystal architecture on the surface of glass. *Sci Rep*. 2016;3(6):36449.
- Savytskii D, Au-Yeung C, Dierolf V, Tamura N, Jain H. Laser fabrication of two-dimensional rotating-lattice single crystal. *Cryst Growth Des*. 2017;17(4):1735–46.
- Pontoni D, Bolze J, Dingenouts N, Narayanan T, Ballauff M. Crystallization of calcium carbonate observed in-situ by combined small- and wide-angle X-ray scattering. *J Phys Chem B*. 2003;107(22):5123–5.
- de Moor P-PEA, Beelen TPM, van Santen RA. In situ observation of nucleation and crystal growth in zeolite synthesis. A small-angle X-ray scattering investigation on Si-TPA-MFI. *J Phys Chem B*. 1999;103(10):1639–50.
- Somani RH, Hsiao BS, Nogales A, Srinivas S, Tsou AH, Sics I, et al. Structure development during shear flow-induced crystallization of i-PP: in-situ small-angle X-ray scattering study. *Macromolecules*. 2000;33(25):9385–94.
- Wilkinson AP, Speck JS, Cheetham AK, Natarajan S, Thomas JM. In situ X-ray diffraction study of crystallization kinetics in  $\text{PbZr}_{1-x}\text{Ti}_x\text{O}_3$ , (PZT,  $x = 0.0, 0.55, 1.0$ ). *Chem Mater*. 1994;6(6):750–4.
- Tamura N, Kunz M, Chen K, Celestre RS, MacDowell AA, Warwick T. A superbend X-ray microdiffraction beamline at the advanced light source. *Mater Sci Eng, A*. 2009;524(1–2):28–32.
- Savytskii D, Sanders M, Golovchak R, Knorr B, Dierolf V, Jain H. Crystallization of stoichiometric  $\text{SbSI}$  glass. *J Am Ceram Soc*. 2014;97(1):198–205.
- Savytskii D, Dierolf V, Tamura N, Jain H. Fabrication of single crystal architecture in  $\text{Sb-S-I}$  glass: transition from dot to line. *J Non Cryst Solids*. 2017;501:43–8. Available from: <http://www.sciencedirect.com/science/article/pii/S0022309317306622>.
- Lee TH, Elliott SR. Ab initio computer simulation of the early stages of crystallization: application to  $\text{Ge}_2\text{Sb}_2\text{Te}_5$  phase-change materials. *Phys Rev Lett*. 2011;107(14):145702.
- Lee TH, Elliott SR. Observing the amorphous-to-crystalline phase transition in  $\text{Ge}_2\text{Sb}_2\text{Te}_5$  non-volatile memory materials from ab initio molecular-dynamics simulations. *Phys Status Solidi B*. 2012;249(10):1886–9.
- Korsunsky AM, Hofmann F, Abbey B, Song X, Belnoue JP, Mocuta C, et al. Analysis of the internal structure and lattice (mis) orientation in individual grains of deformed CP nickel polycrystals



- by synchrotron X-ray micro-diffraction and microscopy. *Int J Fatigue*. 2012;1(42):1–13.
21. Barabash R, Ice GE, Larson BC, Pharr GM, Chung K-S, Yang W. White microbeam diffraction from distorted crystals. *Appl Phys Lett*. 2001;79(6):749–51.
  22. Barabash RI, Ice GE, Larson BC, Yang W. Application of white X-ray microbeams for the analysis of dislocation structures. *Rev Sci Instrum*. 2002;73(3):1652–4.
  23. Budiman A. Probing crystal plasticity at the nanoscales: synchrotron X-ray microdiffraction. Singapore: Springer; 2015 [cited 2018 Oct 3]. (SpringerBriefs in Applied Sciences and Technology). Available from: <http://www.springer.com/us/book/9789812873347>.

## SUPPORTING INFORMATION

Additional supporting information may be found online in the Supporting Information section.

**How to cite this article:** Au-Yeung C, Stan C, Tamura N, Jain H, Dierolf V. In situ study of rotating lattice single-crystal formation in  $\text{Sb}_2\text{S}_3$  glass by Laue  $\mu\text{XRD}$ . *J Am Ceram Soc*. 2019;00:1–8. <https://doi.org/10.1111/jace.16905>